
Article:
Hepach, Helmke, Hughes, Claire orcid.org/0000-0002-9512-8052, Hogg, Karen et al. (2 more authors) (2020) Senescence as the main driver of iodide release from a diverse range of marine phytoplankton. Biogeosciences. 24532020. pp. 2453-2471. ISSN 1726-4189

https://doi.org/10.5194/bg-17-2453-2020

Biogeosciences, 17, 2453–2471, 2020
https://doi.org/10.5194/bg-17-2453-2020

Biogeosciences
Open Access
EGU

Senescence as the main driver of iodide release from a diverse range of marine phytoplankton

Helmke Hepach[1,a,★], **Claire Hughes**[1,★], **Karen Hogg**[2], **Susannah Collings**[1], **and Rosie Chance**[3]

[1]Department of Environment and Geography, University of York, Heslington, York, UK
[2]Department of Biology, University of York, Heslington, York, UK
[3]Wolfson Atmospheric Chemistry Laboratory (WACL), University of York, Heslington, York, UK
[a]now at: RD2, Biological Oceanography, GEOMAR Helmholtz Centre for Ocean Research Kiel, Kiel, Germany
★These authors contributed equally to this work.

Correspondence: Helmke Hepach (hhepach@geomar.de)

Received: 8 November 2019 – Discussion started: 25 November 2019
Revised: 19 February 2020 – Accepted: 18 March 2020 – Published: 7 May 2020

Abstract. The reaction between ozone and iodide at the sea surface is now known to be an important part of atmospheric ozone cycling, causing ozone deposition and the release of ozone-depleting reactive iodine to the atmosphere. The importance of this reaction is reflected by its inclusion in chemical transport models (CTMs). Such models depend on accurate sea surface iodide fields, but measurements are spatially and temporally limited. Hence, the ability to predict current and future sea surface iodide fields, i.e. sea surface iodide concentration on a narrow global grid, requires the development of process-based models. These models require a thorough understanding of the key processes that control sea surface iodide. The aim of this study was to explore if there are common features of iodate-to-iodide reduction amongst diverse marine phytoplankton in order to develop models that focus on sea surface iodine and iodine release to the troposphere. In order to achieve this, rates and patterns of changes in inorganic iodine speciation were determined in 10 phytoplankton cultures grown at ambient iodate concentrations. Where possible these data were analysed alongside results from previous studies. Iodate loss and some iodide production were observed in all cultures studied, confirming that this is a widespread feature amongst marine phytoplankton. We found no significant difference in log-phase, cell-normalised iodide production rates between key phytoplankton groups (diatoms, prymnesiophytes including coccolithophores and phaeocystales), suggesting that a phytoplankton functional type (PFT) approach would not be appropriate for building an ocean iodine cycling model. Iodate loss was greater than iodide formation in the majority of the cultures studied, indicating the presence of an as-yet-unidentified "missing iodine" fraction. Iodide yield at the end of the experiment was significantly greater in cultures that had reached a later senescence stage. This suggests that models should incorporate a lag between peak phytoplankton biomass and maximum iodide production and that cell mortality terms in biogeochemical models could be used to parameterise iodide production.

1 Introduction

Interest in marine inorganic iodine has increased in recent years due to the realisation that ozone deposition to iodide (I^-) at the sea surface plays an important role in ozone cycling and the release of reactive iodine into the troposphere (Carpenter et al., 2013). Once tropospheric ozone reacts with iodide, both hypoiodous acid and molecular iodine are produced in the sea surface microlayer and are then released into the atmosphere (Carpenter et al., 2013; MacDonald et al., 2014):

$$H^+ + I^- + O_3 \rightarrow HOI + O_2, \quad (1)$$

$$H^+ + HOI + I^- \leftrightarrow I_2 + H_2O. \quad (2)$$

Prados-Roman et al. (2015) suggest that up to 75 % of total iodine oxide found in the marine troposphere may originate from this reaction. Once in the troposphere reactive iodine takes part in numerous chemical cycles and reactions

which impact the HO_x and NO_x cycle and ozone cycling (Saiz-Lopez et al., 2012). Iodine is also known to be involved in new particle formation (Ehn et al., 2010; O'Dowd et al., 2002; Sellegri et al., 2016). Ozone deposition to iodide at the sea surface is now considered to be an important component of atmospheric chemistry and is incorporated into large-scale chemical transport models (CTMs; Luhar et al., 2017; Sherwen et al., 2016).

Given the link to atmospheric processes there is now an increased need for accurate maps of global ocean sea surface iodide fields (Carpenter et al., 2013; Helmig et al., 2012). As highlighted by Chance et al. (2014) direct measurements of iodide in surface seawater are sparse. Hence, for the purpose of estimating large-scale ozone deposition and iodine emissions, sea surface iodide concentrations have been estimated as a function of oceanographic variables such as nitrate (Ganzeveld et al., 2009), temperature (Sherwen et al., 2016; Luhar et al., 2017) and chlorophyll *a* (Helmig et al., 2012; Oh et al., 2008) and more recently using combinations of variables (Sherwen et al., 2019). Improving the ability to predict current and future sea surface iodide fields requires the development of process-based models, and that in turn requires a better understanding of the key processes controlling inorganic iodine cycling in marine systems.

Existing measurements show that total inorganic iodine, mainly consisting of iodide and iodate (IO_3^-), is found throughout the oceans at a fairly constant concentration of 450–500 nM (e.g. Elderfield and Truesdale, 1980; Truesdale et al., 2000) but that the ratio of iodide and iodate has considerable spatial variability. In general, iodate occurs at higher concentrations in seawater than iodide throughout most of the water column, but elevated iodide concentrations are found towards the surface (Chance et al., 2010). The highest sea surface iodide concentrations (greater than 100 nM) occur in low-latitude waters, while latitudes greater than about 40° N or S are characterised by concentrations of less than 50 nM (Chance et al., 2014). Chance et al. (2014) also reported that a number of studies have observed a decrease in the proportion of dissolved iodine present as iodate in coastal waters. Given that ozone deposition is proportional to the concentration of iodide at the sea surface (Carpenter et al., 2013), this spatial variability will have a major impact on atmospheric ozone cycling.

Iodide concentrations in seawater are thought to be predominantly controlled by loss due to oxidation to iodate, production due to iodate reduction (see overview – Eq. 3) and physical mixing (reviewed by Chance et al., 2014):

$$IO_3^- + 6H^+ + 6e^- \rightarrow I^- + 3H_2O. \quad (3)$$

The mechanism by which iodate is oxidised to iodide is currently still under debate and highly uncertain. Oxidative species such as hydrogen peroxide or ozone may play a crucial role in this process. Hydrogen peroxide has been suggested to oxidise molecular iodine and then interact with emerging iodide to eventually form iodate (e.g. Truesdale and Moore, 1992). However, the oxidation of iodide to iodate in the mentioned reaction scheme has been postulated to be the slowest among all of the reactions in this scheme occurring in seawater (Wong and Zhang, 1992, and references therein). Furthermore, ozonation has been shown to form iodate from iodide within seconds to minutes (Bichsel and von Gunten, 1999), whereas Teiwes et al. (2019) suggested that hydrated iodide may be oxidised much more effectively to iodate than the bare oxidation of bare iodide, showing that this process is still under debate. There is currently hardly any knowledge if and how this process takes place in natural seawater. Estimates of the lifetime of iodide due to oxidation in natural seawater range between less than 6 months and 40 years (Campos et al., 1996; Edwards and Truesdale, 1997; Tsunogai, 1971). Reported abiotic rates are too slow to explain the shorter lifetimes, so biogenic iodide oxidation driven by phytoplankton (Bluhm et al., 2010) or bacteria (Amachi, 2008; Fuse et al., 2003; Zic et al., 2013) has been suggested, but there remains great uncertainty surrounding this process (Truesdale, 2007). Studies have revealed that both photochemical (Miyake and Tsunogai, 1963; Spokes and Liss, 1996) and biological processes (Bluhm et al., 2010; Chance et al., 2009, 2007; Küpper et al., 1997) are involved in iodate-to-iodide reduction. Calculations suggest that the photochemical reduction of iodate is too slow to be of significance (Truesdale, 2007). Hence we need a greater understanding of biological iodine cycling in order to develop ocean cycling models that can inform studies of ozone deposition to seawater and sea-air iodine emissions.

The reduction of iodate to iodide has been observed in unialgal cultures representative of a wide range of different phytoplankton groups, including diatoms, prymnesiophytes and cyanobacteria (Bluhm et al., 2010; Chance et al., 2007; Moisan et al., 1994; van Bergeijk et al., 2016; Waite and Truesdale, 2003; Wong et al., 2002; see also an overview of rates determined in Table 1). Whilst this demonstrates that the process is widespread amongst marine primary producers, the patterns and rates observed are hugely variable. To date, the highest rates of iodate-to-iodide conversion observed at ambient iodate concentrations (300 nM) have been seen in the cold-water diatom *Nitzschia* sp. (CCMP 580), which has been found to mediate production at 123 amol I^- $cell^{-1}$ d^{-1} (Chance et al., 2007), but there is currently insufficient coverage to establish which (if any) algal groups dominate. There is some evidence to suggest that iodate-to-iodide reduction in marine phytoplankton is to some extent controlled by environmental conditions (e.g. iodate concentration; van Bergeijk et al., 2016), but to date no systematic study has been undertaken to establish the dominant controls. Hence we are unable at present to establish if there are common features of iodate-to-iodide reduction amongst diverse marine phytoplankton or identify the environmental drivers.

The exact processes involved in iodate-to-iodide reduction and its metabolic function (if any) in marine phytoplankton

Table 1. Logarithmic-phase cell-normalised rate of iodate removal and iodide production in a range of marine phytoplankton species investigated in this study and previous studies. Experimental conditions are also listed for comparison. Errors for this study are standard deviations of three replicate cultures.

Algal group	Species (strain)	Growth conditions				Rate (amol cell^{-1} d^{-1})		Source
		IO_3^- (nM)	T (°C)	Light intensity (µmol m^{-2} s^{-1})	Media	IO_3^-	I^-	
Diatoms	*Chaetoceros gelidus* (RCC 4512)	286 ± 7	4	50	K + Si	−4.1 ± 4.6	1.5 ± 1.4	This study
	Chaetoceros sp. (RCC 4208)	280 ± 2	15	75	K + Si	−26.9 ± 1.8	16.6 ± 2.4	This study
	Chaetoceros sp. (CCMP 1690)	297 ± 13	25	100	f/2 + Si	−10.8 ± 1.4	7.9 ± 0.9	This study
	Chaetoceros debilis (EIFEX)	5000	4	50, 100	f/2 + Si	–	16 ± 3, 14 ± 4	Bluhm et al. (2010)
	Nitzschia sp. (CCMP 580)	300 10.3×10^3	4	60	f/2	−148 −6840	123 8600	Chance et al. (2007)
	Thalassiosira pseudonana (CCMP 1335)	300	15	40–50	f/2	−2.18	−1.65	Chance et al. (2007)
	Pseudo-nitzschia turgiduloides (EIFEX)	5000	4	50, 100	f/2 + Si	–	493 ± 182, 643 ± 179	Bluhm et al. (2010)
	Fragilariopsis kerguelensis (EIFEX)	5000	4	50, 100	f/2 + Si	–	80 ± 17, 93 ± 19	Bluhm et al. (2010)
	Eucampia antarctica (CCMP 1452)	5000	4	50, 100	f/2 + Si	–	500 ± 207, 853 ± 124	Bluhm et al. (2010)
	Phaeodactylum tricornutum (CCMP 1055/15)	500 2.5×10^4 2.5×10^6	20	100	f/2	−0.01 −0.4 −38.29	– 10.85 338.3	van Bergeijk et al. (2016)
Prymnesiophytes	*Calcidiscus leptoporus* (RCC 1164)	326 ± 7	20	100	K/2	−114.9 ± 27.6	95.5 ± 19.5	This study
	Gephyrocapsa oceanica (RCC 1318)	284 ± 11	17	25	K/2	−12.0 ± 4.9	2.8 ± 1.6	This study
	Emiliania huxleyi (RCC 1210)	293 ± 20	17	25	K/2	−5.6 ± 3.6	1.3 ± 0.4	This study
	Emiliania huxleyi (RCC 4560)	354 ± 14	20	100	K	−11.0 ± 2.5	0.7 ± 0.6	This study
	Phaeocystis antarctica (RCC 4024)	321 ± 18	4	50	K/2	−5.2 ± 1.1	3.5 ± 0.9	This study
	Phaeocystis sp. (RCC 1725)	273 ± 5	20	100	K/2	−93.9 ± 25.0	60.9 ± 22.5	This study
	Emiliania huxleyi (CCMP 373)	300	15	40–50	f/2	−18	66.3	Chance et al. (2007)
	Emiliania huxleyi (CCMP 371)	5000	18	50, 100	f/2	–	11 ± 2, 9 ± 5	Bluhm et al. (2010)
	Tisochrysis lutea (CCAP927/14)	500 2.5×10^4 2.5×10^6	20	100	f/2	−0.2 −2.4 −91.0	0.7 13.8 195.1	van Bergeijk et al. (2016)
Cyanobacteria	*Synechococcus* sp. (RCC 2366)	341 ± 20	20	100	SN	−2.3 ± 0.3	0.0 ± 0.0	This study

remain uncertain, but suggestions include links with nitrate reductase (Tsunogai and Sase, 1969) and senescence (Bluhm et al., 2010). Indications for the link with nitrate reductase come from correlations between iodide concentration and nitrate reductase activity in the field (Wong and Hung, 2001) and from laboratory studies with enzyme extracts (Hung et al., 2005; Tsunogai and Sase, 1969). There is, however, also evidence from culture studies which suggests that nitrate reductase is not involved in iodate-to-iodide conversion. For instance, Waite and Truesdale (2003) deactivated the nitrate reductase enzyme in a haptophyte species which was still able to reduce iodate to iodide, and Bluhm et al. (2010) did not see a link between iodide production with nitrate limitation in their monoculture studies. They instead suggested a link of iodide production with senescence mediated by reduced sulfur leaked from lysing cells. To date, this was the only study that tied iodide release to a specific growth phase of microalgae. Studies (Küpper et al., 1997, 2008) have suggested that iodate-to-iodide reduction in marine macroalgae is linked to light-induced oxidative stress. Whilst iodide has been shown to control oxidative stress in microalgae (Hernández Javier et al., 2018), a link between iodate reduction and light-induced oxidative stress has yet to be demonstrated in this group of organisms. A better understanding of the purpose and mechanism of iodate-to-iodide reduction in marine phytoplankton would help with the development of process-based models of inorganic iodine cycling in the oceans.

The aim of this study was to establish if there are any general trends of iodate-to-iodide reduction across a diverse range of phytoplankton species to assist with future predictive model development. We studied growth-stage-specific and overall changes in iodate-to-iodide conversion at ambient iodate concentrations (~ 300 nM) in 10 polar, temperate and tropical phytoplankton species from three microalgal groups including diatoms, prymnesiophytes and cyanobacteria. Where possible, we compiled the rates observed with those from the literature to provide an overall view of patterns of iodate-to-iodide conversion across the marine phytoplankton cultures studied to date.

2 Materials and methods

2.1 Phytoplankton strains

The 10 phytoplankton strains (Fig. 1) used in this study were obtained from the Roscoff Culture Collection (RCC) and the National Center for Marine Algae and Microbiota Bigelow (CCMP). The strains include the diatoms (blue shades) *Chaetoceros gelidus* (RCC 4512), *Chaetoceros* sp. (RCC 4208) and *Chaetoceros* sp. (CCMP 1690); the prymnesiophytes (yellow to red shades) *Emiliania huxleyi* (RCC 1210, coccolithophore), *Emiliania huxleyi* (RCC 4560, coccolithophore), *Calcidiscus leptoporus* (RCC 1164, coccolithophore), *Gephyrocapsa oceanica* (RCC 1318, coccolithophore), *Phaeocystis antarctica* (RCC 4024, phaeocystales) and *Phaeocystis* sp. (RCC 1725, phaeocystales); and the cyanobacterium *Synechococcus* sp. (RCC 2366; depicted in dark green). Where we studied strains of the same genus or species, they were from different climate zones. All cultures were non-axenic but checked for bacterial growth in the beginning and the end of the experiments using flow cytometry (see Sect. 2.2.2).

2.2 Experimental set-up

Each strain was grown under the conditions (i.e. temperature, light intensity, media; Table 1) specified by the culture collection from which they were obtained (Fig. 1). All media were prepared in ESAW – enriched seawater, artificial water (Berges et al., 2001), which was autoclaved before use. Concentrations of nutrients in media can be found in Table 2. Handling of all sterile media and cultures was done in a biosafety cabinet to reduce the risk of bacterial contamination. Each experiment included triplicate phytoplankton cultures and triplicate media-only controls. The duration of the experiment was dictated by the growth dynamics of the specific strain. Each experiment was carried out until the respective culture reached the senescent phase, but due to time constraints cultures were at different stages of senescence when each experiment was terminated.

Experiments were performed in either 2 or 4 L borosilicate glass flasks, which contained 1 or 2 L of medium, respectively. The experimental as well as the control flasks were spiked with iodate at a final concentration between 300 and 400 nM (Tables 1 and 2), reflecting lower to average natural concentrations (Chance et al., 2014). Initial iodide concentrations in the flasks ranged on average between 1.32 ± 0.23 nM (*Phaeocystis* sp., RCC 1725) and 20.77 ± 20.49 nM (*Chaetoceros gelidus*, RCC 4521). Iodate solutions were prepared in Milli-Q water using solid potassium iodate (KIO_3; Fisher Scientific, SLR grade, $\geq 99.5\,\%$) and were autoclaved before being added to the ESAW. At the start of each experiment experimental flasks were inoculated with 15–30 mL of stock culture, depending on the stock culture cell density and volume of the flasks. Flasks were then incubated under red and blue LED lights with a 12 h : 12 h light–dark cycle in a temperature-controlled room. Regular (weekly or bi-weekly) sampling was performed for inorganic iodine species (I^-, IO_3^-), cell counts and in vivo chlorophyll fluorescence readings. Methods used for the determination of these parameters are described in Sect. 2.2.1 to 2.2.2.

2.2.1 Determination of iodide and iodate

Samples for iodide and iodate analyses were gently hand-filtered through a 25 mm GF/F (Whatman) filter into sterile 15 mL falcon tubes and then stored at $-20\,^{\circ}$C until further analysis within 6 months of collection. Our storage tests re-

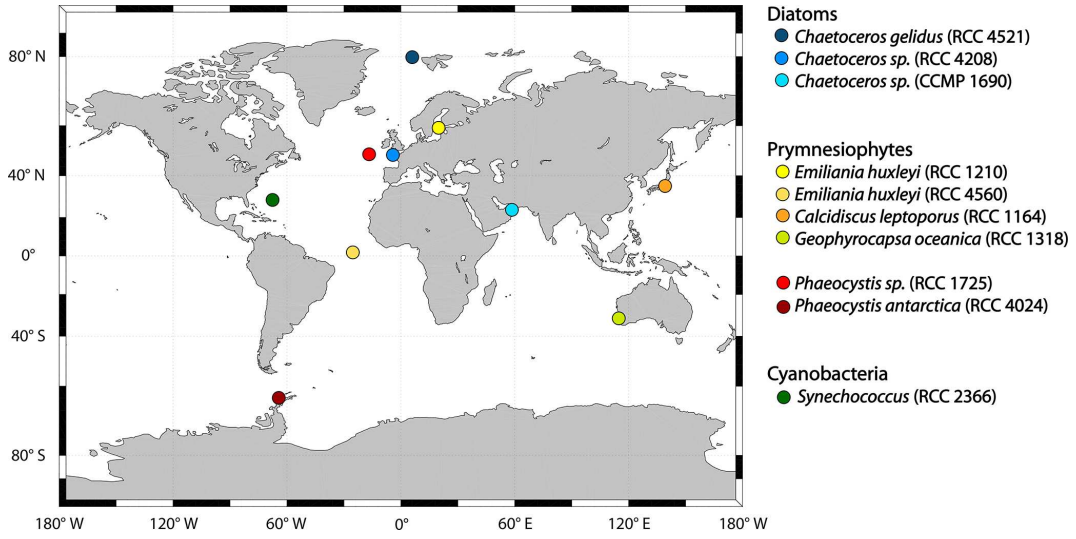

Figure 1. All strains used in the incubation experiments and the original location where they were isolated. Blue colours indicate strains that belong to the group diatoms, yellow to red refers to strains from the class of prymnesiophytes (yellow to orange denotes species from the order of coccolithophores, while red stands for species from the order of phaeocystales) and dark green refers to the only cyanobacteria studied here, *Synechococcus* sp.

Table 2. Overview of results for the control data for the incubation experiments. Start and end points are shown for each measured parameter per type of medium. Values shown are mediums and standard deviations derived from all replicates. Media-only controls were carried out for each incubation set-up with three replicates each and were treated the same way as the inoculated flasks. No significant variations between start and end points were detected in any of the parameters shown with respect to detection limits and precision of the methods. Note that the standard deviations from start and end points are within measurement precision. Additionally, start concentrations of nutrients for each medium are shown (NO_3^- – nitrate, PO_4^{3-} – phosphate, SIO_3^{2-} – silicate, NH_4^+ – ammonium). Please note that concentrations of these nutrients were not measured but correspond to the concentrations as stated in the original publications for these media (K; K/2; K + Si: Keller et al., 1987; f/2: Guillard and Ryther, 1962; SN: Waterbury et al., 1986).

Medium	Time point	IO_3^- (nM)	I^- (nM)	NO_3^- (µM)	PO_4^{3-} (µM)	SiO_3^{2-} (µM)	NH_4^+ (µM)
f/2 + Si	Start	295.8 ± 6.7	3.3 ± 0.7	882.0	36.2	106.0	
	End	304.2 ± 26.2	3.7 ± 2.1				
K/2	Start	236.5 ± 55.4	2.7 ± 0.7	441.0	5.0		25.1
	End	237.4 ± 37.5	2.9 ± 0.3				
K	Start	245.6 ± 27.87	2.2 ± 0.9	882.0	10.0		50.1
	End	247.3 ± 13.9	9.8 ± 0.4				
K + Si	Start	251.5 ± 38.9	2.8 ± 0.7	882.0	10.0	106.0	50.1
	End	249.5 ± 35.5	4.6 ± 0.3				
SN	Start	327.9 ± 35.7	4.5 ± 2.1	9000.0	9.9		
	End	323.1 ± 27.0	11.6 ± 3.8				

vealed that inorganic iodine speciation was maintained during this period of storage.

Iodide analysis was performed using cathodic stripping square-wave voltammetry as described in Campos (1997) using a Metrohm voltammeter and NOVA software. The sample volume was 12 mL, and nitrogen was used as purging gas to remove oxygen; 90 µL of 0.2 % Triton X-100 was added to the sample before purging to increase the sensitivity of the method. Quantification of iodide was achieved by performing standard additions. Potassium iodide (KI; Acros Organics, extra pure, trace metal basis, 99.995 %) standards were prepared in Milli-Q water with a final concentration of about 1×10^{-5}–2×10^{-5} M. Final concentrations were determined by applying linear regression. Precision of the technique was 5 %–10 % based on repeat measurements of aliquots from the same sample.

Iodate was determined spectrophotometrically according to Truesdale and Spencer (1974) using a PerkinElmer

Lambda 35 UV/Vis spectrometer with a 1 cm quartz cuvette. During analysis 50 µL of 1.5 M sulfamic acid (Fisher Scientific, analytical reagent grade, $\geq 99.9\,\%$) was added to 2.3 mL of sample, and absorbance at 350 nm was measured after 1 min. Following this, 150 µL of 0.6 M KI solution was added and mixed, and the absorbance at 350 nm was read after 2.5 min. Quantification was achieved by performing a standard curve on every measurement day using potassium iodate (see Sect. 2.2) in Milli-Q water. Final iodate concentrations were then retrieved using the difference of the second reading and the first reading and by linear regression from the standards. Sample precision was between 5 % and 10 % based on regular measurements of triplicates from the same sample. A standard in the measured concentration range was measured every five samples to determine the daily instrumental drift.

2.2.2 Biological measurements: in vivo chlorophyll fluorescence and cell counts

In vivo chlorophyll fluorescence was measured at every sampling point for each culture and control replicate. A sample of 5 mL was transferred into a 1 cm cuvette, and fluorescence (excitation / emission: 460 nm / 685 nm) was measured using a Turner Trilogy Designs fluorometer.

Automated cell counts were performed using a Vi-CELL XR (Beckman Coulter); 500 µL of the sample was transferred into a vial. The Vi-CELL takes up the sample and mixes it 1 : 1 with trypan blue; dead cells take up the dye, while live cells do not, and deliver it to a flow cell for camera imaging, where differences in grey scale between the live and dead cell are determined by the software. Fifty images were analysed to determine the cell concentration and viability. The ESAW sample had to be acidified with 5 µL of concentrated hydrochloric acid directly prior injecting into the Vi-CELL due to the alkaline nature of the trypan blue and consequential precipitation of sea salt that complicated the measurement using the Vi-CELL without pre-acidification. Pre-tests with acidification and in vivo chlorophyll fluorescence of different algal cultures showed no change in the fluorescence with pre-acidification in this short time period. The precision of these measurements was on average 10 %, determined from triplicates from the same culture. No cells were detected in the control treatments. Bacterial contamination was evaluated using flow cytometry. Samples were stained with DAPI (1 µg mL^{-1}) for 30 min at room temperature and analysed using a CytoFLEX S cytometer (Beckman Coulter), using an event rate of less than 1000 events per second, at flow rate of 60 µL min^{-1} for a minimum of 1 min. DAPI was excited using the 405 nm laser and emitted photons detected in the wavelength range 450/50 nm. A sterile sample diluent buffer was used to set the detection threshold, and a sterile medium was used as a negative control.

2.3 Calculations and data analysis

Iodide production and iodate incorporation rates were calculated from slopes applying linear regression analysis of iodide and iodate concentration versus time according to Bluhm et al. (2010). Pearson's linear correlation coefficients (R^2) were generally larger or equal to 0.7, with the exception of one culture replicate of *Emiliania huxleyi* (RCC 4566), where R^2 was 0.5. Iodine production and incorporation rates per cell were normalised to time-averaged cell numbers.

All statistical tests applied in this study were conducted in MATLAB® and SigmaPlot Version 13. Datasets that were correlated to each other were first tested for normal distribution using the Liliefors test. Depending on the outcome of the test, linearity was calculated using the Pearson's linear correlation coefficient (R) or the Spearman's ρ (r_s). The significance level applied here was $p \leq 0.05$. Further statistical tests applied include the t test, the two-sided Wilcoxon rank sum test and one-way ANOVAs. One-way ANOVAs were used when the means of more than two datasets were investigated at the same time.

Normal distribution of datasets used in the one-way ANOVAs was tested using the Shapiro–Wilk test. Since most datasets were not normally distributed, we performed Kruskal–Wallis one-way ANOVAs, since they require neither normal distribution nor equal variances. The specific purpose of each test is introduced at relevant points in Sect. 3.

3 Results and discussion

The results of the phytoplankton growth curve experiments are summarised in Figs. 2–5. It can be seen that a decline in iodate concentrations and increase in iodide were detected in all strains studied. Concentrations of iodide in the media-only controls (Table 2) were very close to the detection limit, and thus the small changes observed are within our measurement error (please note: the standard deviation here represents the variation between culture replicates). Additionally, any changes in iodate observed in the controls were within the precision of the spectrometric method. This confirms that the observed changes in inorganic iodine in the cultures were biologically mediated. It is apparent from Figs. 2–5 that there is variability in the time series and magnitude of changes in iodate and iodide concentrations between cultures, but growth rates, biomass levels and the growth stage reached also differed between strains. The data are explored further in Sect. 3.1 to 3.3 to identify if any common features or patterns of inorganic iodine speciation change can be identified once these other factors are taken into account.

This study did not set out to identify the mechanism of iodate-to-iodide conversion in marine phytoplankton, but we can say that it is unlikely that nitrate reductase (Hung et al., 2005) was the mechanism responsible. It was postulated that the responsible enzyme switches to iodate once nitrate is de-

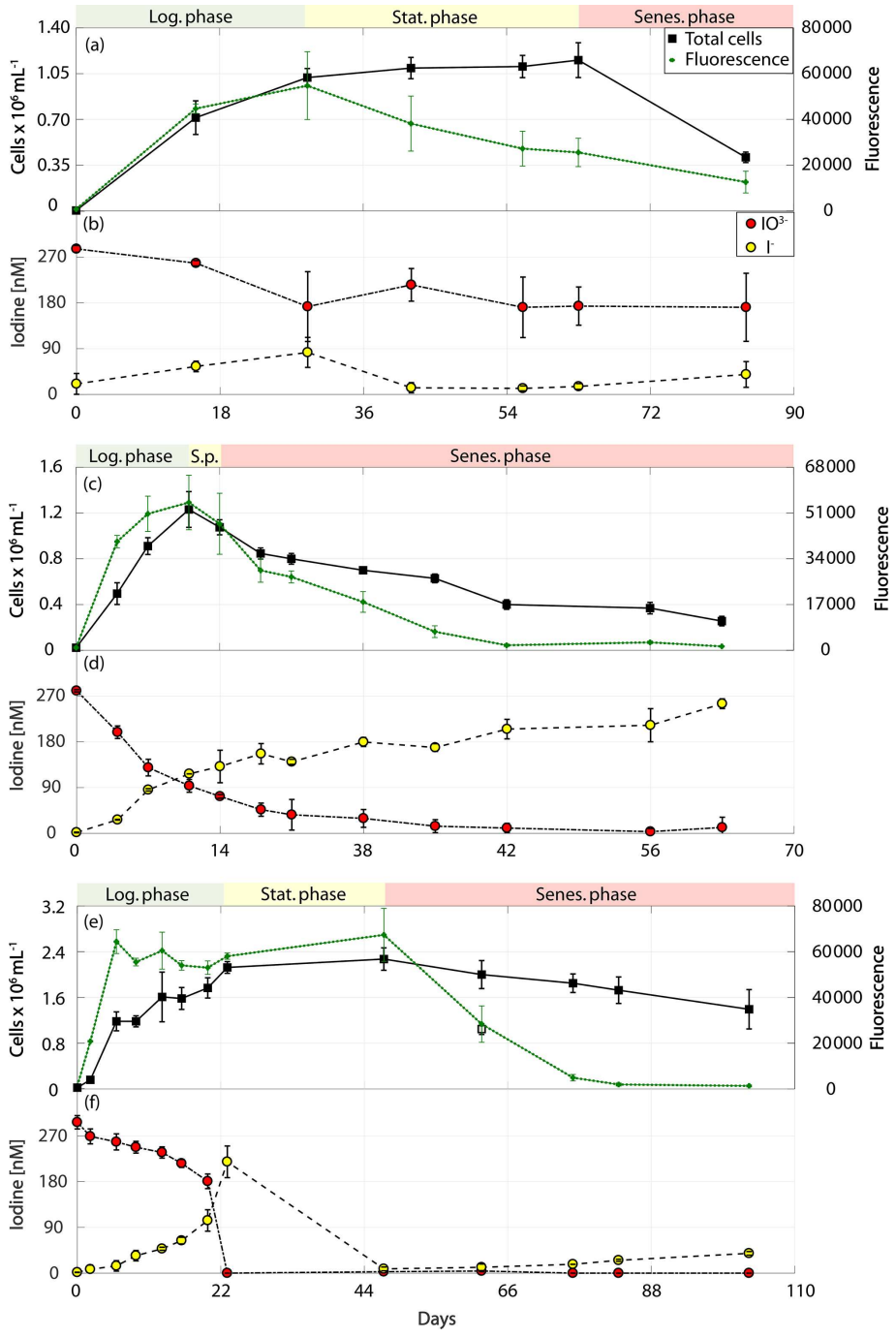

Figure 2. Total cell counts (black – total) and fluorescence readings (green) as well as inorganic iodine speciation (red – iodate, yellow – iodide) over the course of the growth curve experiments of diatoms for *Chaetoceros gelidus* (RCC 4512) in **(a)** and **(b)**, *Chaetoceros* sp. (RCC 4208) in **(c)** and **(d)**, and *Chaetoceros* sp. (CCMP 1690) in **(e)** and **(f)**. The colour-shaded bars on top of each graph indicate where the logarithmic phase (green), the stationary phase (yellow) and the senescent phase (red) began and ended based on total cell counts and fluorescence. Values depicted are means from culture replicates, with error bars indicating the standard deviations of these means.

pleted (Tsunogai and Sase, 1969). Media that used to grow each strain in this study, however, contain high levels of nitrate (see Table 2), so the cultures were not limited in this nutrient at the beginning of the experiments, when production of iodide could already be observed. The other proposed mechanism for iodate reduction to iodide involves the release of reduced sulfur during the senescence phase (Bluhm et al., 2010). Our further analysis in Sect. 3.1 to 3.3 explores the im-

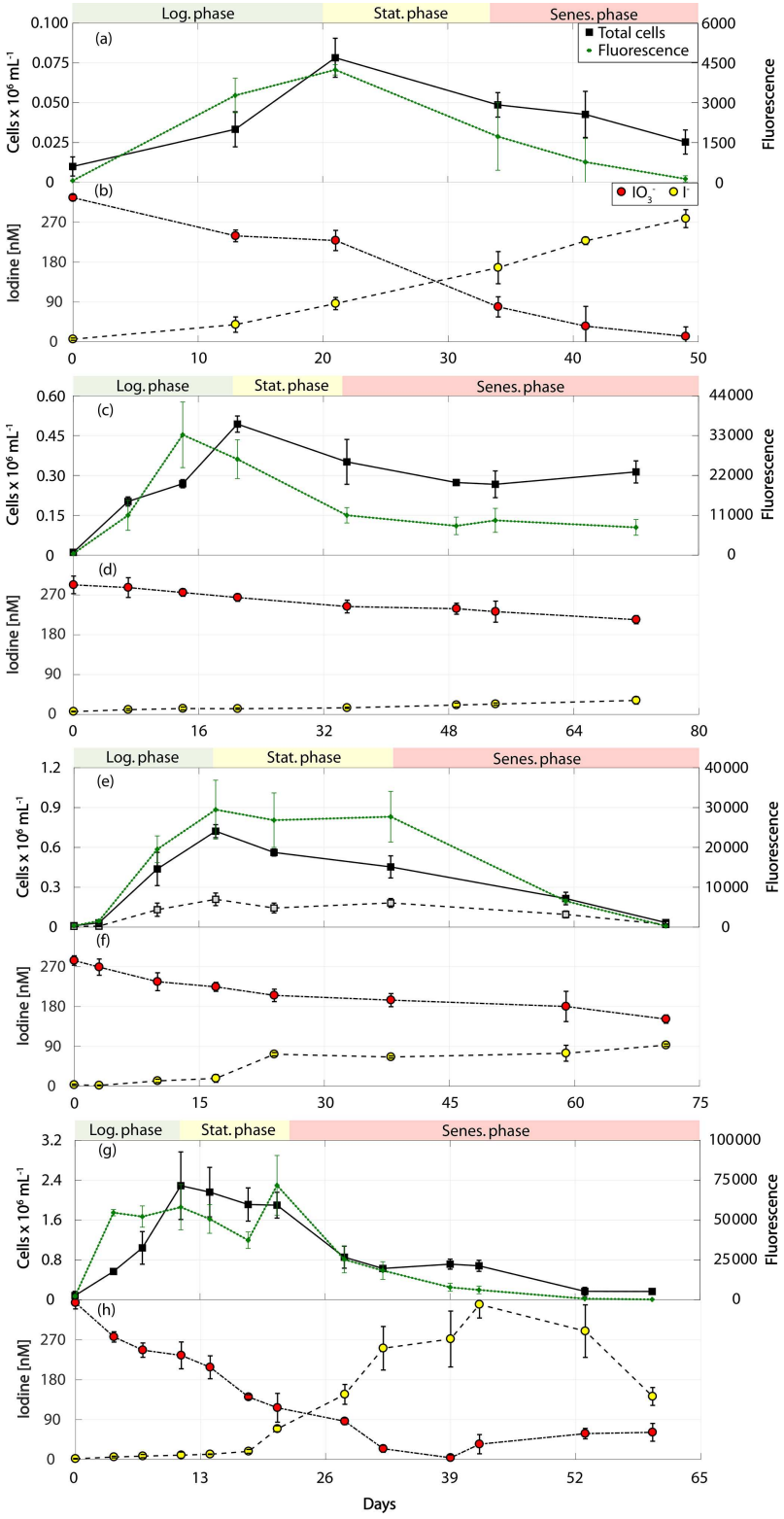

Figure 3. Total cell counts (black – total) and fluorescence readings (green) as well as inorganic iodine speciation (red – iodate, yellow – iodide) over the course of the growth curve experiments of calcifying prymnesiophytes for *Calcidiscus leptoporus* (RCC 1164) in **(a)** and **(b)**, *Emiliania huxleyi* (RCC 1210) in **(c)** and **(d)**, *Gephyrocapsa oceanica* (RCC 1318) in **(e)** and **(f)**, and *Emiliania huxleyi* (RCC 4560) in **(g)** and **(h)**. The colour-shaded bars on top of each graph indicate where the logarithmic phase (green), the stationary phase (yellow) and the senescent phase (red) began and ended based on total cell counts. Values depicted are means from culture replicates, with error bars indicating the standard deviations of these means.

portance of the growth stage on changes in inorganic iodine speciation and hence in some way explores if the mechanism described in Bluhm et al. (2010) can explain the observed changes.

3.1 Logarithmic stage rates of iodate-to-iodide reduction

3.1.1 Cell-normalised rates

Log-phase, cell-normalised iodide production rates were calculated (Table 1) to assess if normalising to biomass allows any patterns to be identified across phytoplankton strains. Our rates are presented in Table 1 alongside those reported in previous studies for comparison. Rates observed in *Synechococcus* sp. (RCC 2366) are not discussed further here, as it was the only cyanobacterium strain studied. Overall we observed the highest rate of iodide production (95.5 ± 19.5 amol I^- cell^{-1} d^{-1}) in the prymnesiophyte *Calcidiscus leptoporus* (RCC 1164). The warm-water (20 °C) *Phaeocystis* sp. (RCC 1725) also had high rates of change of inorganic iodine speciation (60.9 ± 22.5 amol I^- cell^{-1} d^{-1}), but the cold-water *Phaeocystis antarctica* (RCC 4024) had relatively lower rates (3.5 ± 0.9 amol I^- cell^{-1} d^{-1}). The *Emiliania huxleyi* strains investigated here (RCC 1210, RCC 4560) were both found to drive low rates of change in inorganic iodine speciation (< 2 amol I^- cell^{-1} d^{-1}). Other studies have found rates of iodide production in *Emiliania huxleyi* of 66.3 amol I^- cell^{-1} d^{-1} (CCMP 373, 300 nM iodate; Chance et al., 2007) and 9 ± 5 to 11 ± 2 amol I^- cell^{-1} d^{-1} (CCMP 371, at 5 µM iodate; Bluhm et al., 2010). The only other Prymnesiophyte investigated to date (*Tisochrysis lutea*, CCAP927/14) has been found to produce iodide at rates of 0.7 amol I^- cell^{-1} d^{-1}at 500 nM iodate and 195.1 nM iodate at 2.5 mM (van Bergeijk et al., 2016).

For the sake of comparability, we concentrate only on studies that reported iodide production and iodate consumption rates normalised to phytoplankton cell numbers in the following. Across all studies on iodate-to-iodide reduction by phytoplankton undertaken to date that also include phytoplankton cell numbers, the highest rates of iodide production have been observed in diatoms, but this was not the case in our study. The highest rate of iodide increase we observed amongst the diatoms studied was in the temperate *Chaetoceros* sp. (RCC 4208; 16.6 ± 2.4 amol I^- cell^{-1} d^{-1}). Relatively lower rates were observed in the other two cold-water and temperate *Chaetoceros* strains (Table 1: *Chaetoceros gelidus*, RCC 4512; *Chaetoceros* sp., CCMP 1690). Similar low rates have been found in other marine diatoms (e.g. *Phaeodactylum tricornutum*, CCMP 1055/15; van Bergeijk et al., 2016), and some diatom cultures (e.g. *Thalassiosira pseudonana*, CCMP 1335; Chance et al., 2007) have not been found to mediate iodate-to-iodide reduction at all. Previous studies have found some diatom species to be among the main producers of iodide. The cold-water *Nitzschia* sp. (CCMP 580) has been found to mediate 123 amol I^- cell^{-1} d^{-1} at 300 nM iodate (Chance et al., 2007). The very high rates of diatom iodate-to-iodide conversion reported in Table 1 from other studies were observed when the cultures were presented with super-ambient concentrations of iodate (e.g. *Nitzschia* sp., CCMP 580, 8600 amol I^- cell^{-1} d^{-1} at 10 µM iodate; Chance et al., 2007; *Pseudo-nitzschia turgiduloides*, 643 ± 179 amol I^- cell^{-1} d^{-1}; *Fragilariopsis kerguelensis*, 93 ± 19 amol I^- cell^{-1} d^{-1}, both at 5 µM iodate; Bluhm et al., 2010). Whilst the increased iodate-to-iodide reduction at the higher levels of iodate is of interest, such rates are unlikely to occur in the natural environment, especially since iodide release rates have been shown to increase with increasing initial iodate concentrations (e.g. Wong et al., 2002; van Bergeijk et al., 2016). A similar wide range in iodide production and iodate consumption rates was found for monoculture batch experiments where no cell-normalised rates were presented (Butler et al., 1981; Moisan et al., 1994; Wong et al., 2002; Waite and Truesdale, 2003). For example, while Wong et al. (2002) present high iodide production rates in monocultures of the green alga *Dunaliella tertiolecta*, Butler et al. (1981) did not see any changes in iodide levels in their experiments with the same species.

Overall, when all cell-normalised iodide production rates for all strains studied to date are brought together (this study and rates from the literature), there is no clear difference between phytoplankton groups (where there are sufficient data to make comparisons). For diatoms, rates at ambient levels of iodate (300–500 nM) range from -1.65 amol I^- cell^{-1} d^{-1} in *Thalassiosira pseudonana* (CCMP 1335; Chance et al., 2007) to 123 amol I^- cell^{-1} d^{-1} in *Nitzschia* sp. (CCMP 580; Chance et al., 2007). In the prymnesiophytes, rates range from 0.7 ± 0.6 amol I^- cell^{-1} d^{-1} in *Emiliania huxleyi* (RCC 4560; this study) to 95.5 ± 19.5 amol I^- cell^{-1} d^{-1} in *Calcidiscus leptoporus* (RCC 1164; this study) at ambient iodate. There was no significant difference in iodide production rates between diatoms and prymnesiophytes (Mann–Whitney rank sum test: $p > 0.05$, $n = 20$ for diatoms and $n = 22$ for prymnesiophytes) or between diatoms, prymnesiophytes and phaeocystales (Kruskal–Wallis: $p > 0.05$, $n = 20$ for diatoms, $n = 15$ for prymnesiophytes and $n = 6$ for phaeocystales) when data from this study and previous studies are considered together. These results were the same whether only data from experiments conducted at ambient iodate were included or data from all experiments (including those at super-ambient iodate levels) were considered.

3.1.2 Iodine-to-carbon ratios

An alternative way to compare iodide production rates between species and groups is to normalise against activity, such as the carbon-fixation rate, rather than cell density. As the photosynthetic rate was not measured, we use known literature values for cellular carbon (Table 3) to calculate

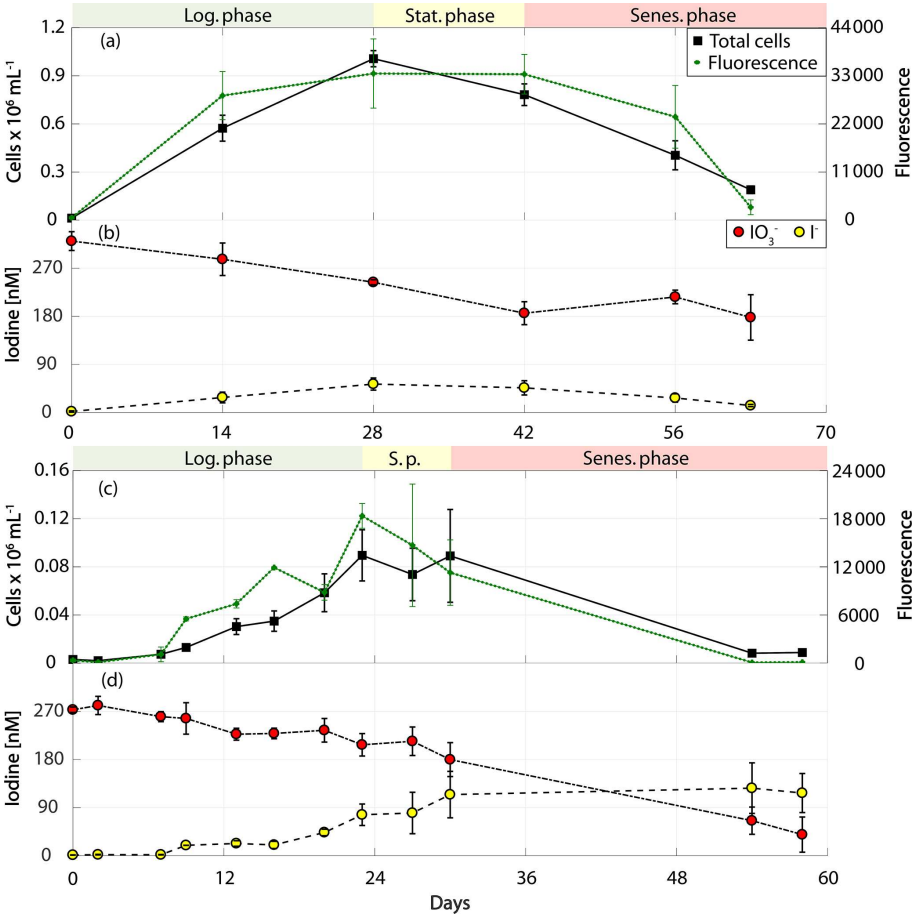

Figure 4. Total cell counts (black – total) and fluorescence readings (green) as well as inorganic iodine speciation (red – iodate, yellow – iodide) over the course of the growth curve experiments of prymnesiophytes for *Phaeocystis antarctica* (RCC 4024) in **(a)** and **(b)** and *Phaeocystis* sp. (RCC 1725) in **(c)** and **(d)**. The colour-shaded bars on top of each graph indicate where the logarithmic phase (green), the stationary phase (yellow) and the senescent phase (red) began and ended based on total cell counts. Values depicted are means from culture replicates, with error bars indicating the standard deviations of these means.

Table 3. Ratios of IO_3^- removal and I^- production to increase in cellular carbon (net primary production – NPP). Also presented are the cellular carbon levels used to make these calculations. Errors are the standard deviations of three replicate cultures.

	Species (strain)	pg C cell^{-1}	IO_3^- : C	SD	I^- : C	SD
Diatoms	*C. gelidus* (RCC 4512)	8.2[a]	4.2×10^{-4}	2.2×10^{-4}	7.1×10^{-5}	6.2×10^{-5}
	Chaetoceros sp. (RCC 4208)	8.2[a]	2.3×10^{-4}	2.8×10^{-5}	1.5×10^{-4}	4.4×10^{-5}
	Chaetoceros sp. (CCMP 1690)	8.2[a]	8.4×10^{-5}	3.0×10^{-5}	2.0×10^{-5}	1.2×10^{-5}
Prymnesiophytes	*Calcidiscus leptoporus* (RCC 1164)	32.5[b]	5.3×10^{-4}	9.0×10^{-5}	4.5×10^{-4}	1.2×10^{-4}
	Gephyrocapsa oceanica (RCC 1318)	13.8[c]	7.4×10^{-5}	2.6×10^{-5}	1.8×10^{-5}	1.0×10^{-5}
	Emiliania huxleyi (RCC 1210)	10.7[d]	6.5×10^{-5}	4.0×10^{-5}	1.5×10^{-5}	5.7×10^{-6}
	Emiliania huxleyi (RCC 4560)	10.7[d]	6.1×10^{-5}	1.5×10^{-5}	3.8×10^{-6}	3.1×10^{-6}
	Phaeocystis antarctica (RCC 4024)	9.0[e]	1.0×10^{-4}	1.6×10^{-5}	6.8×10^{-5}	1.3×10^{-5}
	Phaeocystis sp. (RCC 1725)	9.0[e]	8.1×10^{-4}	3.1×10^{-4}	1.1×10^{-3}	4.7×10^{-4}
Cyanobacteria	*Synechococcus* sp. (RCC 2366)	0.3[f]	2.7×10^{-3}	2.2×10^{-4}	2.9×10^{-5}	2.3×10^{-5}

[a] Degerlund et al. (2012). [b] Heinle (2013). [c] Jin et al. (2013), Baumann (2004). [d] Blanco-Ameijeiras et al. (2016). [e] Vogt et al. (2012). [f] Buitenhuis et al. (2012).

log-phase rates of carbon incorporation into cellular biomass (equivalent to net primary production – NPP). These rates are then used to calculate the molar ratio of iodate removed or iodide-produced (I : C) conversion ratios for each phytoplankton strain used in this study. Ratios are presented in Table 3 and vary between 10^{-6} and 10^{-3} for I : C. The range of rates found in this study are variable but do encompass the I : C ratios found in field studies, which are on the order of 10^{-4} (Chance et al., 2010; Elderfield and Truesdale, 1980; Wong et al., 1976). With our estimated I : C ratios lying within the ranges reported from field studies, it can be assumed that the processes that we observe in our monoculture studies are likely transferable to the field. Whilst there are insufficient data to undertake statistical analysis, it is clear that, as with the cell-normalised rates, the I : C in diatoms and phaeocystales / coccolithophores overlap significantly. Amongst the diatoms, the I : C ratio ranged from 2.0×10^{-5} ($\pm 1.2 \times 10^{-5}$) in *Chaetoceros* sp. (CCMP 1680) to 1.5×10^{-4} ($\pm 4.4 \times 10^{-5}$) in *Chaetoceros* sp. (RCC 4208). In the prymnesiophytes it was found to range from 1.5×10^{-5} ($\pm 5.7 \times 10^{-6}$) in *Emiliania huxleyi* (RCC 1210) to 1.1×10^{-3} ($\pm 4.7 \times 10^{-4}$) in *Phaeocystis* sp. (RCC 1725). The highest I : C amongst the coccolithophores was 4.5×10^{-4} ($\pm 1.2 \times 10^{-4}$) in *Calcidiscus leptoporus* (RCC 1164).

3.1.3 Relationship between iodate uptake and iodide production

Figure 6 shows the relationship between the log-phase iodate removal and iodide production rates in 30 phytoplankton cultures from our study and an additional 11 strains from two studies (Chance et al., 2007; Wong et al., 2002), in which the cultures were also supplied with ambient iodate concentrations. Note, however, that we were not able to identify any studies where initial iodate was introduced to the cultures in the ambient level that also covered the growth stages beyond the log phase. Thus, only cultures from this study were included in Fig. 6b. Log-phase iodate consumption and iodide production rates correlate significantly (Fig. 6a; Spearman's rank: $r_s = -0.37$, $p = 0.018$, $n = 41$), but the correlation for the overall experimental rates is stronger (Fig. 6b; Spearman's rank: $r_s = -0.72$, $p = 0.000$, $n = 30$). Also shown in the figure are the 1 : 1 lines. Data points below the line suggest higher iodate removal rates than iodide production, while data points above suggest the opposite. Data points below the line after the end of the experiments (Fig. 6b) indicate loss of iodine during the experiment (or missing iodine). A least-squares regression line on top of the 1 : 1 line would indicate that all iodate consumed is converted into iodide in the majority of the cultures. The flatter slope of the regression line (grey line) in Fig. 6a in comparison to that in Fig. 6b suggests higher incorporation of iodate compared to iodide production during the logarithmic phase. This implies that iodate taken up during active growth is not immediately converted to iodide. Whilst the slope is steeper, the least-squares regression line in Fig. 6b still does not sit over the 1 : 1 line, suggesting incomplete conversion of iodate to iodide and missing iodine. The existence of missing iodine is explored further in Sect. 3.3.

3.2 Comparison of log-phase and post-log-phase rates of iodide production

To investigate if the growth stage is an important determinant of the rates of inorganic iodine speciation across diverse phytoplankton groups, we compared logarithmic and post-logarithmic rates of change in iodide (Fig. 7). It is clear from Fig. 7 that there is no general pattern across the strains studied. Of the 30 cultures studied, 14 demonstrated higher iodide production rates in the log phase and 16 in the post-log phase. A paired t test revealed that there was no consistent difference between log- and post-log-phase rates of change in iodide across the phytoplankton strains included in this study ($p > 0.05$, $n = 30$).

It is interesting to note that declines in iodide concentrations were observed during the post-log phase in two strains (*Chaetoceros* sp., CCMP 1680, -2.6 ± 0.5 amol I^- cell^{-1} d^{-1}; *Phaeocystis antarctica*, RCC 4024, -1.1 ± 1.4 amol I^- cell^{-1} d^{-1}). There is also evidence from the growth curve data that there was a decline in iodide concentrations during the later stages of the growth curve experiment for *Emiliania huxleyi* (RCC 4560; Fig. 3). It has been established in previous studies that phytoplankton also takes up iodide (de la Cuesta and Manley, 2009; Bluhm et al., 2010; van Bergeijk et al., 2013), and this could explain these declines. Two of the cultures (*Chaetoceros* sp., CCMP 1690 – Fig. 2; *Emiliania huxleyi*, RCC 4560 – Fig. 3) had very low iodate (< 10 nM) during the period when iodide concentrations decreased, so the cultures may have switched their iodine source to iodide. However, one of the cultures where a decline was observed (*Phaeocystis antarctica*, RCC 4024 – Fig. 4) still had substantial levels of iodate (~ 180 nM) when iodide decline was observed. In addition to uptake the disappearance of iodide may have also indicated conversion into other organic or inorganic forms. Volatile or low-molecular-weight organoiodine compounds are usually found in concentrations in the picomolar range both in monocultures (Hughes et al., 2006) and in the field (Hepach et al., 2016). Dissolved organic iodine (DOI) has been suggested to be a possible intermediate step in the reduction of iodate to iodide. DOI is found in nanomolar ranges in coastal regions with high riverine input, but concentrations are lower in open ocean regions (Wong and Cheng, 2001). To date, evaluations of DOI in monocultural batch experiments have not been conducted. However, Wong and Cheng (2001) suggested that DOI could form from microalgal exudates, which could, for example, apply to species such as *Phaeocystis* sp.

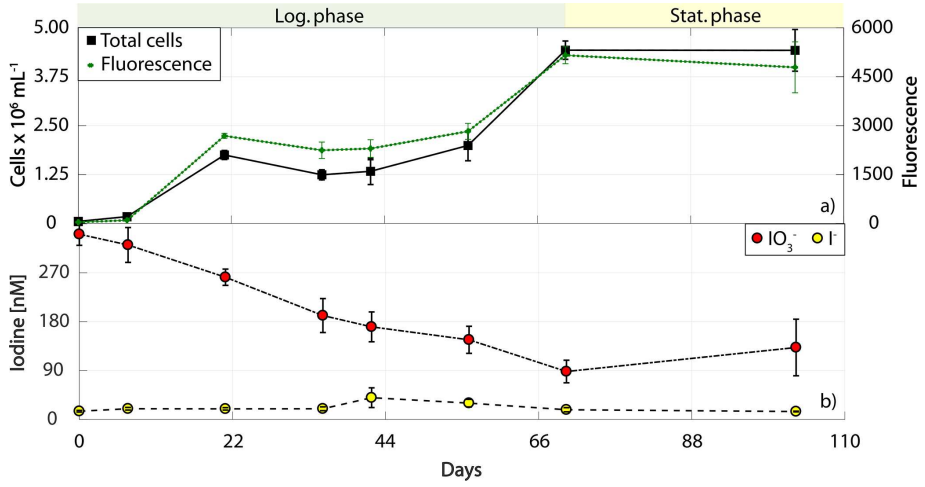

Figure 5. Total cell counts (black – total) and fluorescence readings (green) as well as inorganic iodine speciation (red – iodate, yellow – iodide) over the course of the growth curve experiments of *Synechococcus* sp. (RCC 2366). The colour-shaded bars on top of each graph indicate where the logarithmic phase (green) and the stationary phase (yellow) started and ended based on total cell counts. Values depicted are means from culture replicates, with error bars indicating the standard deviations of these means.

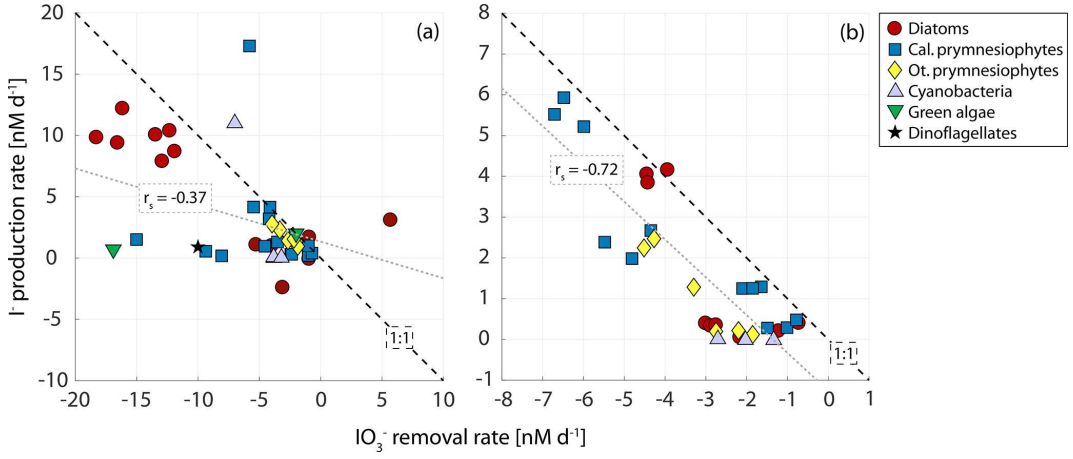

Figure 6. Relationship between **(a)** IO_3^- removal and I^- production rate, including other studies with similar initial IO_3^- concentrations (Chance et al., 2007; Wong et al., 2002) during the logarithmic growth phase, and **(b)** the overall (whole experiment) removal and production rates in the 30 phytoplankton cultures (three cultures per strain) from only this study (note: we were not able to find studies of iodide production that were conducted over all growth phases of the cultures and that additionally were carried out with iodate at ambient levels; thus only our cultures are included). Rates are calculated as the change in the inorganic iodine species normalised to experimental duration. Dashed line is the 1 : 1 line. Grey lines are the least-square lines ($p = 0.018$, $n = 41$; $p = 0.00001$, $n = 30$). The marker symbol gives information on whether the shown culture was a diatom (circle), calcifying prymnesiophyte (square), other prymnesiophytes (diamond), cyanobacteria (upward-pointing triangle), green algae (downward-pointing triangle) or dinoflagellate (star). Note that the calcifying prymnesiophyte outlier in **(a)** is from Chance et al. (2007), in which the I^- production rate for *Emiliania huxleyi* (CCMP 373) in the log phase was calculated over the course of fewer days than the IO_3^- consumption rate due to loss of I^- during the log phase.

3.3 Net changes in iodine speciation across experimental duration

The rates of change (normalised to the total experimental duration) and composition of iodine speciation at the end of the experiments in each replicate are shown in Fig. 8. The largest overall net decrease in iodate (mean ± standard deviation from the culture set-up; -313.2 ± 18.1 nM) was seen in *Calcidiscus leptoporus*, while the smallest (-78.6 ± 26.1 nM) was seen in *Emiliania huxleyi* (RCC 1210). Consistent with this, Fig. 8a shows that the largest overall rate of decline in iodate was observed in *Calcidiscus leptoporus* (-6.4 ± 0.4 nM d^{-1}), with the smallest again seen in *Emiliania huxleyi* (RCC 1210; -1.1 ± 0.4 nM d^{-1}). The highest net increase in iodide was seen in *Calcidiscus lepto-*

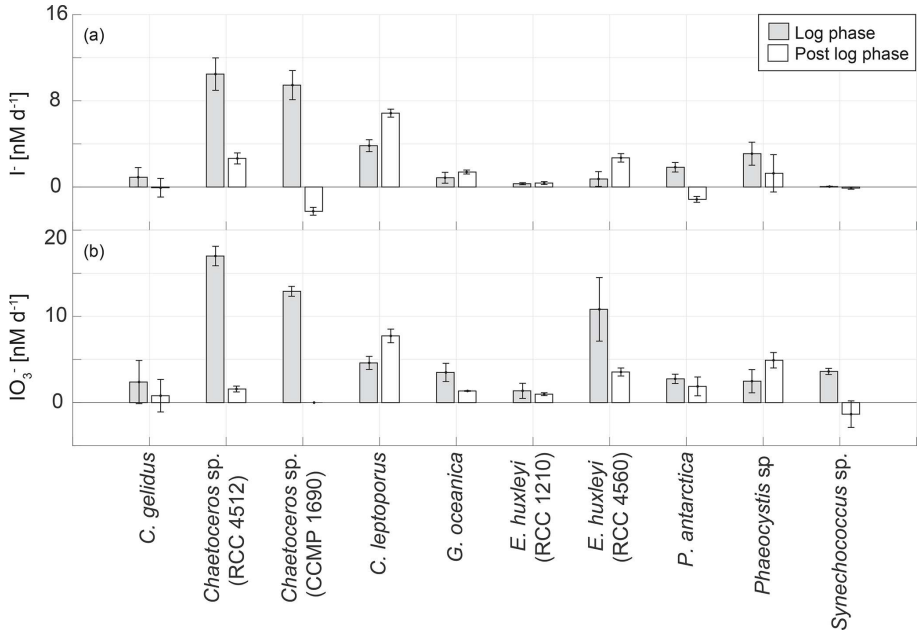

Figure 7. Comparison of the average net change in **(a)** I^- and **(b)** IO_3^- concentrations during logarithmic (light grey bar) and post-logarithmic (white bar) stages of growth in 10 marine phytoplankton cultures averaged over the length of the respective growth phase. Error bars show the standard deviation from three replicate cultures.

porus (RCC 1164; 272.3 ± 17.6 nM), and the lowest was seen in *Synechococcus* sp., in which some changes in inorganic iodine speciation were observed, but no significant net increase in iodide was observed across the experiment (-0.5 ± 1.3 nM). The highest overall rates of iodide increase (Fig. 8a) were observed in *Calcidiscus leptoporus* (5.6 ± 0.4 nM d^{-1}), and the lowest were observed in *Synechococcus* sp. (0.0 ± 0.0 nM d^{-1}).

Figure 8b shows the composition of iodine speciation at the end of each experiment, with blue bars indicating missing iodine (difference of net iodate decline and iodide increase). It is apparent that in 23 of the 30 studied culture replicates, there is significant missing iodine (i.e. less iodide produced compared to iodate lost from the media). Here "significant" is defined as more than 10 % of initial iodate, given that 10 % is the precision of the measurement (see Sect. 2.2.1). In 8 out of 30 replicates, this missing iodine is more than 50 % of the initial iodate concentrations. The missing iodine levels range from 46.9 ± 33.3 nM in *Emiliania huxleyi* (RCC 1210) to 257.8 ± 10.9 nM in *Chaetoceros* sp. (CCMP 1690). This suggests that there is not always an immediate conversion of iodate to iodide in the medium and that some of the iodate taken up is retained by the cells or converted into (and stored) another form. Previous studies have also observed missing iodine in its phytoplankton cultures (Chance et al., 2007; van Bergeijk et al., 2016; Wong et al., 2002). It is possible that the missing iodine was converted into organic forms (including volatile organics); other inorganic forms such as hypoiodous acid and molecular iodine, which, however, are very short-lived in the ocean due to reaction with, for example, organic matter (Luther et al., 1995); or particulate iodine. Establishing the location or form of the missing iodine will require confirmation from future studies which include measurements of all forms of iodine (iodate, iodide, particulate iodine, volatile organoiodine compounds, DOI, molecular iodine and hypoiodous acid). Another explanation for missing iodine is the storage of iodine as iodate, iodide or another form in the cell itself, which is released after a certain trigger. For example, the release of stored iodine compounds has been linked to light stress in macro-algae (e.g. Küpper et al., 1997). Overall observations of missing iodine are not consistent with the mechanism of iodate reduction to iodide proposed by Bluhm et al. (2010), who suggested that iodate discharged during the senescent phase is converted to iodide in the external media following the release of reduced sulfur species upon cell lysis. This conclusion is based on the fact that we found iodide release during all stages of growth and that iodate is taken up and not immediately transformed into iodide, as would be expected from the mechanism proposed by Bluhm et al. (2010). However, our study shows that senescence plays a significant role in releasing iodide to some extent. Assuming that missing iodine is linked to storage of iodide in the cells themselves, cell senescence could still play a significant role in releasing iodide in the latter stages of growth, which would also explain why missing iodine decreases with progressing stage of senescence.

It is apparent from Figs. 2–5 that although each culture had entered the senescence stage by the end of the experi-

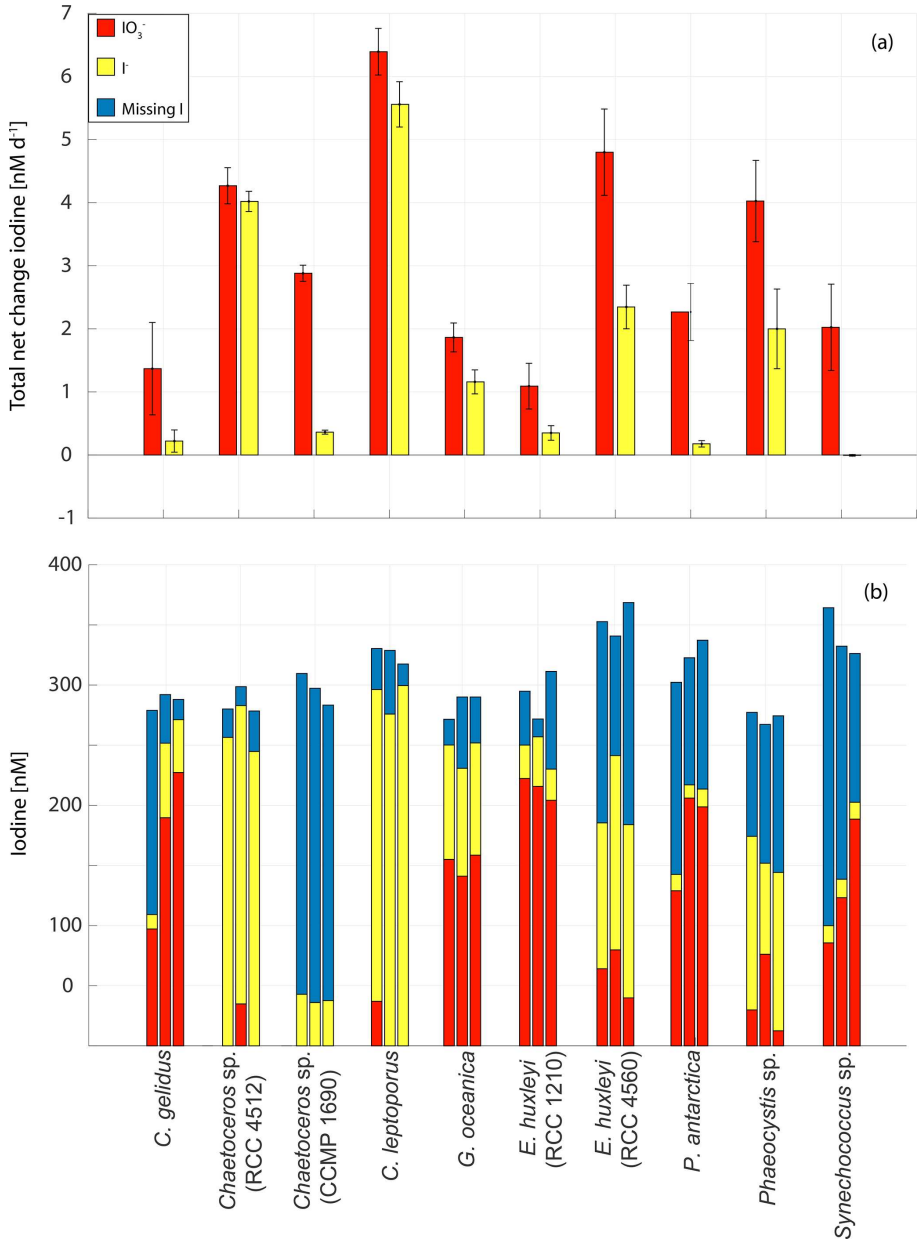

Figure 8. Changes in inorganic iodine speciation in 10 marine phytoplankton cultures: **(a)** overall (whole experiment) rate of change in IO_3^- (red) and I^- (yellow) normalised for the duration of each experiment. Error bars show the standard deviation of three replicate cultures and **(b)** total IO_3^- (red bar), I^- (yellow bar) and missing iodine (blue bar) for all three replicates for each experiment at the end of each experiment.

ment, the length of time spent in this stage and the proportion of dead cells present varied between experiments. Given the potential for a link between iodate reduction and cell death (Bluhm et al., 2010), it is important to consider this when exploring differences in the net changes in inorganic iodine speciation across the experimental duration. Figure 9 presents the ratio of iodide produced to iodate taken up ($I^- : IO_3^-$), average rate of change in iodide across the experimental duration and the net increase in iodide produced across each experiment grouped by senescence stage. Here the senescence stage is defined as the percentage of maximum cells remaining at the end of the experiment, and the two groups are late senescence (0 %–50 % cells remaining) and early senescence (51 %–100 % cells remaining). Figure 9a shows that there is a significant difference in $I^- : IO_3^-$ (Wilcoxon rank sum test: $p = 0.014$, $n = 30$, significance level $p < 0.05$). The average $I^- : IO_3^-$ (Fig. 9a) is significantly higher in cultures at a late stage of senescence (median of ratio is 0.57) com-

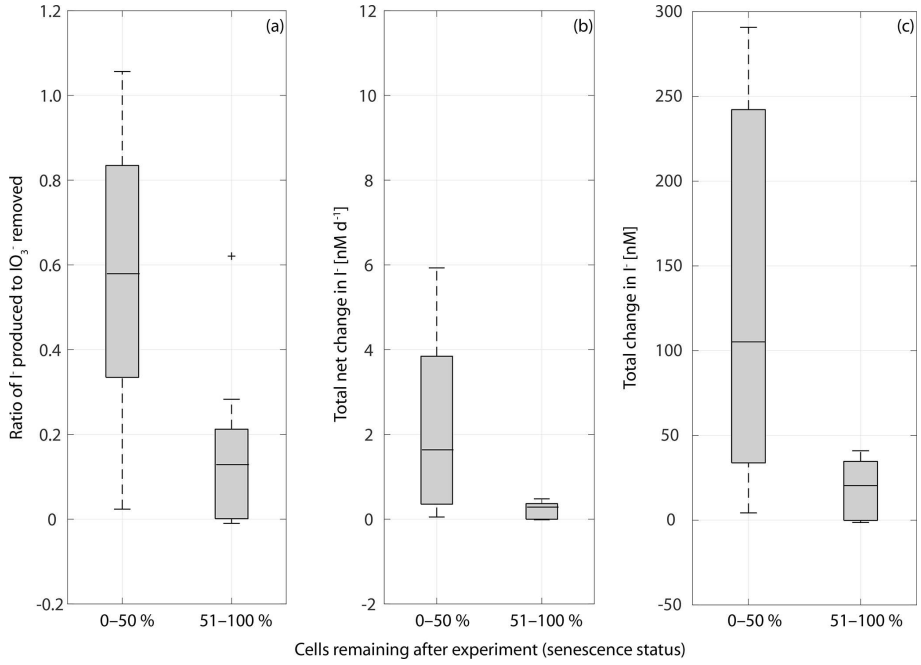

Figure 9. Box plot of the ratio of I^- produced to IO_3^- removed in cultures of a range of marine phytoplankton at different stages of senescence in **(a)**, net rate of change in iodine over the whole length of the experiment **(b)** and the total change in iodide at the end of each experiment **(c)**. Senescence status is defined as the percentage of the maximum cell number remaining at the end of the experiment: 0 %–50 % indicates that there are 0 %–50 % of cells remaining indicating late senescence, and a senescence status of 51 %–100 % indicates that there are 51 %–100 % of cells remaining indicating early senescence. Ratios are significantly different between the 0 %–50 % and 51 %–100 % groups (Wilcoxon rank sum test: $p = 0.014$, $n = 30$), as is the total net iodine change ($p = 0.005$, $n = 30$) and the total change in iodide ($p = 0.006$, $n = 30$).

pared to those in early senescence (median of ratio is 0.12). This suggests that across a diverse range of phytoplankton cells, a greater proportion of the iodate taken up is released as iodide as senescence progresses. This is supported by the Wilcoxon rank sum tests performed on the average rate of change in iodide across senescent stage groups ($p = 0.005$, $n = 30$; Fig. 9b) and total net change in iodide ($p = 0.006$, $n = 30$). The link with cell senescence would not have been apparent from the log or post-log analysis (Sect. 3.2), as this did not consider senescence stage. Although our observations do not support the idea that immediate conversion of iodate to iodide is the dominant production process, this analysis still suggests that there is some link to senescence, which needs to be explored in further studies. For example, cell lysis may cause stored iodide to diffuse into the medium.

Overall our findings suggest that cell death is an important factor controlling iodide production. Considering this and the observation of missing iodine across all phytoplankton groups, we propose that phytoplankton takes up or converts iodate to other organic or inorganic forms during active growth and that the taken-up or converted iodate is reduced or released to iodide during cell death or senescence. Part of the reduction that occurs upon cell death could be explained by the reduced sulfur mechanism proposed by Bluhm et al. (2010), but our results suggest that there will be a myriad of other chemical changes that could occur as cells lyse that could also be involved. Iodide production during the active growth (log) phase can be explained by the low level of cell death that is known to take place even during active growth. Whilst the environmental stress (e.g. nutrient availability) that occurs in a batch culture over time will clearly enhance the rate of cell death, natural cell death due to (for example) exhaustion of division potential (age) or programmed cell death can occur at any time (Franklin et al., 2010). Assuming that iodide could be stored within the cells, the release of iodine during earlier growth phases could also be a response of algal cells to changing ambient parameters such as light or temperature.

3.4 Implications for process-based models of inorganic iodine cycling in the oceans

The incorporation of phytoplankton functional types (PFTs) into the ecosystem dynamics of ocean biogeochemical models has led to improved performance and accuracy (Gregg et al., 2003), but our results suggest that this approach would not be suitable for models of inorganic iodine cycling in seawater. Representatives of common PFTs, including pico-autotrophs (e.g. cyanobacteria), phytoplankton silicifiers (e.g. diatoms) and phytoplankton calcifiers (e.g. coccolithophores; Quéré et al., 2005), have been investigated for iodate-to-iodide conversion here and in previous studies. Fol-

lowing the definition in Quéré et al. (2005) each PFT in an inorganic iodine cycling model would need to have a distinct and explicit role. However in the present study all PFTs studied to date were found to drive iodate-to-iodide reduction, there was large variability in rates within PFTs, and we did not find a significant difference in rates of conversion between diatoms and prymnesiophytes or diatoms, coccolithophores and phaeocystales. The available evidence suggests that there is no significant difference in the rates and patterns of iodate-to-iodide reduction between phytoplankton groups or functional types.

Our observations of missing iodine and a link between iodide production and cell senescence do, however, provide important guidance for ocean iodine cycling models. These findings suggest that highest iodide release rates will be observed during the later stages of phytoplankton blooms, and there will most likely be a lag between maximal phytoplankton biomass and the highest iodide concentrations. This suggestion is supported by time-series measurements in coastal Antarctica (2005–2008, Chance et al., 2010) which show that each year there was a time lag of around 60 d between the onset of the microalgal bloom and the iodide maximum. These results suggest that the terms for (non-predatory) phytoplankton mortality typically included in biogeochemical models (e.g. ERSEM; Butenschön et al., 2016) could be used to incorporate iodide production into process-based models.

4 Conclusions

This study aimed to establish if there are common features of iodate-to-iodide reduction amongst diverse phytoplankton that could be used to guide the development of ocean iodine cycling models. By combining our results with those of previous studies, we have shown that there is no significant difference in cell-normalised iodide production rates between key phytoplankton groups (diatoms versus prymnesiophytes) or phytoplankton functional types (PFTs; e.g. diatoms versus coccolithophores). We did, however, observe missing iodine in the majority of phytoplankton cultures studied and found that the iodide yield is significantly higher in cultures at a later senescence stage. Resolving the fate of missing iodine, which could be different forms of iodine or storage of iodine compounds within the cells themselves, may yield useful information on the mechanisms behind iodate conversion to iodide. Furthermore, in line with a previous time-series study (Chance et al., 2010), these findings suggest that there will be a lag between maximum iodide release rates and peaks in phytoplankton biomass and productivity in marine systems. We propose that process-based models of inorganic iodine cycling could be linked to marine ecosystem models via the phytoplankton mortality term. Future process studies should focus on whether different environmental and physiological drivers of cell death influence the iodide yield.

Data availability. The underlying data of this study can be accessed at the British Oceanographic Data Centre (BODC) with the following https://doi.org/10.5285/a3ca5dd8-9e06-06be-e053-6c86abc02d35 (last access: 21 April 2020, Hepach and Hughes, 2020).

Author contributions. CH designed the experiments together with HH and RC. HH conducted the experiments and prepared the paper together with CH. CH provided essential input for the preparation of this paper and was a PI of the NERC project "Iodide in the ocean: distribution and impact on iodine flux and ozone loss". Please note that HH and CH contributed equally to this paper. KH provided methodological knowledge for microalgal cell counts and provided input during the paper preparation. SC contributed to completing the incubation experiments. RC provided methodological knowledge regarding iodine measurement methods and provided input during paper preparation.

Competing interests. The authors declare that they have no conflict of interest.

Acknowledgements. This study was funded by NERC as part of the project "Iodide in the ocean: distribution and impact on iodine flux and ozone loss". We would like to thank Liselotte Tinel for her scientific and technical input during iodine analysis and Matt Pickering for technical help during the incubation experiments.

Financial support. This research has been supported by the Natural Environment Research Council (grant no. NE/N009983/1).

Review statement. This paper was edited by Koji Suzuki and reviewed by two anonymous referees.

References

Amachi, S.: Microbial contribution to global iodine cycling: Volatilization, accumulation, reduction, oxidation, and sorption of iodine, Microbes Environ., 23, 269–276, https://doi.org/10.1264/jsme2.ME08548, 2008.

Baumann, K. H.: Importance of size measurements for coccolith carbonate flux estimates, Micropaleontology, 50, 35-43, https://doi.org/10.2113/50.Suppl_1.35, 2004.

Berges, J. A., Franklin, D. J., and Harrison, P. J.: Evolution of an artificial seawater medium: Improvements in enriched seawater, artificial water over the last two decades, J. Phycol., 37, 1138–1145, https://doi.org/10.1046/j.1529-8817.2001.01052.x, 2001.

Bichsel, Y. and von Gunten, U.: Oxidation of Iodide and Hypoiodous Acid in the Disinfection of Natural Waters, Environ. Sci. Technol., 33, 4040–4045, https://doi.org/10.1021/ess990336c, 1999.

Blanco-Ameijeiras, S., Lebrato, M., Stoll, H. M., Iglesias-Rodriguez, D., Muller, M. N., Mendez-Vicente, A.,

and Oschlies, A.: Phenotypic variability in the coccolithophore emiliania huxleyi, PLoS One, 11, 1–17, https://doi.org/10.1371/journal.pone.0157697, 2016.

Bluhm, K., Croot, P., Wuttig, K., and Lochte, K.: Transformation of iodate to iodide in marine phytoplankton driven by cell senescence, Aquat. Biol., 11, 1–15, https://doi.org/10.3354/ab00284, 2010.

Buitenhuis, E. T., Li, W. K. W., Vaulot, D., Lomas, M. W., Landry, M. R., Partensky, F., Karl, D. M., Ulloa, O., Campbell, L., Jacquet, S., Lantoine, F., Chavez, F., Macias, D., Gosselin, M., and McManus, G. B.: Picophytoplankton biomass distribution in the global ocean, Earth Syst. Sci. Data, 4, 37–46, https://doi.org/10.5194/essd-4-37-2012, 2012.

Butenschön, M., Clark, J., Aldridge, J. N., Allen, J. I., Artioli, Y., Blackford, J., Bruggeman, J., Cazenave, P., Ciavatta, S., Kay, S., Lessin, G., van Leeuwen, S., van der Molen, J., de Mora, L., Polimene, L., Sailley, S., Stephens, N., and Torres, R.: ERSEM 15.06: a generic model for marine biogeochemistry and the ecosystem dynamics of the lower trophic levels, Geosci. Model Dev., 9, 1293–1339, https://doi.org/10.5194/gmd-9-1293-2016, 2016.

Butler, E. C. V., Smith, J. D., and Fisher, N. S.: Influence of phytoplankton on iodine speciation in seawater, Limnol. Oceanogr., 26, 382–386, https://doi.org/10.4319/lo.1981.26.2.0382, 1981.

Campos, M., Farrenkopf, A. M., Jickells, T. D., and Luther, G. W.: A comparison of dissolved iodine cycling at the bermuda atlantic time-series station and hawaii ocean time-series station, Deep-Sea Res. Pt. II, 43, 455–466, https://doi.org/10.1016/0967-0645(95)00100-x, 1996.

Campos, M. L. A. M.: New approach to evaluating dissolved iodine speciation in natural waters using cathodic stripping voltammetry and a storage study for preserving iodine species, Mar. Chem., 57, 107–117, https://doi.org/10.1016/S0304-4203(96)00093-X, 1997.

Carpenter, L. J., MacDonald, S. M., Shaw, M. D., Kumar, R., Saunders, R. W., Parthipan, R., Wilson, J., and Plane, J. M. C.: Atmospheric iodine levels influenced by sea surface emissions of inorganic iodine, Nat. Geosci., 6, 108–111, https://doi.org/10.1038/ngeo1687, 2013.

Chance, R., Malin, G., Jickells, T., and Baker, A. R.: Reduction of iodate to iodide by cold water diatom cultures, Mar. Chem., 105, 169–180, https://doi.org/10.1016/j.marchem.2006.06.008, 2007.

Chance, R., Baker, A. R., Küpper, F. C., Hughes, C., Kloareg, B., and Malin, G.: Release and transformations of inorganic iodine by marine macroalgae, Estuar. Coast. Shelf Sci., 82, 406–414, https://doi.org/10.1016/j.ecss.2009.02.004, 2009.

Chance, R., Weston, K., Baker, A. R., Hughes, C., Malin, G., Carpenter, L., Meredith, M. P., Clarke, A., Jickells, T. D., Mann, P., and Rossetti, H.: Seasonal and interannual variation of dissolved iodine speciation at a coastal antarctic site, Mar. Chem., 118, 171–181, https://doi.org/10.1016/j.marchem.2009.11.009, 2010.

Chance, R., Baker, A. R., Carpenter, L., and Jickells, T. D.: The distribution of iodide at the sea surface, Environm. Sci., 16, 1841–1859, https://doi.org/10.1039/c4em00139g, 2014.

de la Cuesta, J. L. and Manley, S. L.: Iodine assimilation by marine diatoms and other phytoplankton in nitrate-replete conditions, Limnol. Oceanogr., 54, 1653–1664, https://doi.org/10.4319/lo.2009.54.5.1653, 2009.

Degerlund, M., Huseby, S., Zingone, A., Sarno, D., and Landfald, B.: Functional diversity in cryptic species of chaetoceros socialis lauder (bacillariophyceae), J. Plankton Res., 34, 416–431, https://doi.org/10.1093/plankt/fbs004, 2012.

Edwards, A. and Truesdale, V. W.: Regeneration of inorganic iodine species in loch etive, a natural leaky incubator, Estuar. Coast. Shelf Sci., 45, 357–366, https://doi.org/10.1006/ecss.1996.0185, 1997.

Ehn, M., Vuollekoski, H., Petaja, T., Kerminen, V. M., Vana, M., Aalto, P., de Leeuw, G., Ceburnis, D., Dupuy, R., O'Dowd, C. D., and Kulmala, M.: Growth rates during coastal and marine new particle formation in western ireland, J. Geophys. Res.-Atmos., 115, D18218, https://doi.org/10.1029/2010jd014292, 2010.

Elderfield, H. and Truesdale, V. W.: On the biophilic nature of iodine in seawater, Earth Planet. Sci. Lett., 50, 105–114, https://doi.org/10.1016/0012-821x(80)90122-3, 1980.

Franklin, D. J., Steinke, M., Young, J., Probert, I., and Malin, G.: Dimethylsulphoniopropionate (dmsp), dmsp-lyase activity (dla) and dimethylsulphide (dms) in 10 species of coccolithophore, Mar. Ecol.-Prog. Ser., 410, 13–23, https://doi.org/10.3354/meps08596, 2010.

Fuse, H., Inoue, H., Murakami, K., Takimura, O., and Yamaoka, Y.: Production of free and organic iodine by roseovarius spp, FEMS Microbiol. Lett., 229, 189–194, https://doi.org/10.1016/s0378-1097(03)00839-5, 2003.

Ganzeveld, L., Helmig, D., Fairall, C. W., Hare, J., and Pozzer, A.: Atmosphere-ocean ozone exchange: A global modeling study of biogeochemical, atmospheric, and waterside turbulence dependencies, Global Biogeochem. Cy., 23, GB4021, https://doi.org/10.1029/2008gb003301, 2009.

Gregg, W. W., Ginoux, P., Schopf, P. S., and Casey, N. W.: Phytoplankton and iron: Validation of a global three-dimensional ocean biogeochemical model, Deep-Sea Res. Pt. II, 50, 3143–3169, https://doi.org/10.1016/j.dsr2.2003.07.013, 2003.

Guillard, R. R. and Ryther, J. H.: Studies of marine planktonic diatoms, 1. Cyclotella nana hustedt, and detonula confervacea (cleve) gran, Can. J. Microbiol., 8, 229–239, https://doi.org/10.1139/m62-029, 1962.

Heinle, M.: The effects of light, temperature and nutrients on coccolithophores and implications for biogeochemical models, PhD, School of Environmental Sciences, University of East Anglia, Norwich, 226 pp., 2013.

Helmig, D., Lang, E. K., Bariteau, L., Boylan, P., Fairall, C. W., Ganzeveld, L., Hare, J. E., Hueber, J., and Pallandt, M.: Atmosphere-ocean ozone fluxes during the texaqs 2006, stratus 2006, gomecc 2007, gasex 2008, and amma 2008 cruises, J. Geophys. Res.-Atmos., 117, D04305, https://doi.org/10.1029/2011jd015955, 2012.

Hepach, H. and Hughes, C.: Monoculture experiments of iodate-to-iodide conversion in phytoplankton between November 2016–October 2017, BODC, available at: https://doi.org/10.5285/a3ca5dd8-9e06-06be-e053-6c86abc02d35 last access: 21 April 2020.

Hepach, H., Quack, B., Tegtmeier, S., Engel, A., Bracher, A., Fuhlbrügge, S., Galgani, L., Atlas, E. L., Lampel, J., Frieß, U., and Krüger, K.: Biogenic halocarbons from the Peruvian upwelling region as tropospheric halogen source, Atmos. Chem. Phys., 16, 12219–12237, https://doi.org/10.5194/acp-16-12219-2016, 2016.

Hernández Javier, L. H., Benzekri, H., Gut, M., Claros, M. G., van Bergeijk, S., Canavate, J. P., and Manchado, M.: Characterization of iodine-related molecular processes in the marine microalga tisochrysis lutea (haptophyta), Front. Mar. Sci., 5, 134, https://doi.org/10.3389/fmars.2018.00134, 2018.

Hughes, C., Malin, G., Nightingale, P. D., and Liss, P. S.: The effect of light stress on the release of volatile iodocarbons by three species of marine microalgae, Limnol. Oceanogr., 51, 2849–2854, https://doi.org/10.4319/lo.2006.51.6.2849, 2006.

Hung, C. C., Wong, G. T. F., and Dunstan, W. M.: Iodate reduction activity in nitrate reductase extracts from marine phytoplankton, B. Mar. Sci., 76, 61–72, 2005.

Jin, P., Gao, K. S., and Beardall, J.: Evolutionary responses of a coccolithophorid gephyrocapsa oceanica to ocean acidification, Evolution, 67, 1869–1878, https://doi.org/10.1111/evo.12112, 2013.

Keller, M. D., Selvin, R. C., Claus, W., and Guillard, R. R. L.: Media for the culture of oceanic ultraphytoplankton, J. Phycol., 23, 633–638, https://doi.org/10.1111/j.1529-8817.1987.tb04217.x, 1987.

Küpper, F. C., Schweigert, N., Ar Gall, E., Potin, P., Vilter, H., and Kloareg, B.: Iodine uptake in laminariales involves extracellular, haloperoxidase-mediated oxidation of iodide, Phycologia, 36, 56–56, https://doi.org/10.1007/s004250050469, 1997.

Küpper, F. C., Carpenter, L. J., McFiggans, G. B., Palmer, C. J., Waite, T. J., Boneberg, E. M., Woitsch, S., Weiller, M., Abela, R., Grolimund, D., Potin, P., Butler, A., Luther, G. W., Kroneck, P. M. H., Meyer-Klaucke, W., and Feiters, M. C.: Iodide accumulation provides kelp with an inorganic antioxidant impacting atmospheric chemistry, P. Natl. Acad. Sci. USA, 105, 6954–6958, https://doi.org/10.1073/pnas.0709959105, 2008.

Luhar, A. K., Galbally, I. E., Woodhouse, M. T., and Thatcher, M.: An improved parameterisation of ozone dry deposition to the ocean and its impact in a global climate-chemistry model, Atmos. Chem. Phys., 17, 3749–3767, https://doi.org/10.5194/acp-17-3749-2017, 2017.

Luther, G. W., Wu, J. F., and Cullen, J. B.: Redox chemistry of iodine in seawater – frontier molecular-orbital theory considerations, in: Aquatic chemistry: Interfacial and interspecies processes, edited by: Huang, C. P., Omelia, C. R., and Morgan, J. J., Advances in chemistry series, Amer. Chemical Soc., Washington, 135–155, 1995.

MacDonald, S. M., Gómez Martín, J. C., Chance, R., Warriner, S., Saiz-Lopez, A., Carpenter, L. J., and Plane, J. M. C.: A laboratory characterisation of inorganic iodine emissions from the sea surface: dependence on oceanic variables and parameterisation for global modelling, Atmos. Chem. Phys., 14, 5841–5852, https://doi.org/10.5194/acp-14-5841-2014, 2014.

Miyake, Y. and Tsunogai, S.: Evaporation of iodine from ocean, J. Geophys. Res., 68, 3989–3993, https://doi.org/10.1029/JZ068i013p03989, 1963.

Moisan, T. A., Dunstan, W. M., Udomkit, A., and Wong, G. T. F.: The uptake of iodate by marine-phytoplankton, J. Phycol., 30, 580–587, https://doi.org/10.1111/j.0022-3646.1994.00580.x, 1994.

O'Dowd, C. D., Hameri, K., Makela, J., Vakeva, M., Aalto, P., de Leeuw, G., Kunz, G. J., Becker, E., Hansson, H. C., Allen, A. G., Harrison, R. M., Berresheim, H., Geever, M., Jennings, S. G., and Kulmala, M.: Coastal new particle formation: Environmental conditions and aerosol physicochemical characteristics during nucleation bursts, J. Geophys. Res.-Atmos., 107, D198107, https://doi.org/10.1029/2000jd000206, 2002.

Oh, I. B., Byun, D. W., Kim, H. C., Kim, S., and Cameron, B.: Modeling the effect of iodide distribution on ozone deposition to seawater surface, Atmos. Environ., 42, 4453–4466, https://doi.org/10.1016/j.atmosenv.2008.02.022, 2008.

Prados-Roman, C., Cuevas, C. A., Hay, T., Fernandez, R. P., Mahajan, A. S., Royer, S.-J., Galí, M., Simó, R., Dachs, J., Großmann, K., Kinnison, D. E., Lamarque, J.-F., and Saiz-Lopez, A.: Iodine oxide in the global marine boundary layer, Atmos. Chem. Phys., 15, 583–593, https://doi.org/10.5194/acp-15-583-2015, 2015.

Quéré, C. L., Harrison, S. P., Colin Prentice, I., Buitenhuis, E. T., Aumont, O., Bopp, L., Claustre, H., Cotrim Da Cunha, L., Geider, R., Giraud, X., Klaas, C., Kohfeld, K. E., Legendre, L., Manizza, M., Platt, T., Rivkin, R. B., Sathyendranath, S., Uitz, J., Watson, A. J., and Wolf-Gladrow, D.: Ecosystem dynamics based on plankton functional types for global ocean biogeochemistry models, Global Change Biol., 11, 2016–2040, https://doi.org/10.1111/j.1365-2486.2005.1004.x, 2005.

Saiz-Lopez, A., Plane, J. M. C., Baker, A. R., Carpenter, L. J., von Glasow, R., Martin, J. C. G., McFiggans, G., and Saunders, R. W.: Atmospheric chemistry of iodine, Chem. Rev., 112, 1773–1804, https://doi.org/10.1021/cr200029u, 2012.

Sellegri, K., Pey, J., Rose, C., Culot, A., DeWitt, H. L., Mas, S., Schwier, A. N., Temime-Roussel, B., Charriere, B., Saiz-Lopez, A., Mahajan, A. S., Parin, D., Kukui, A., Sempere, R., D'Anna, B., and Marchand, N.: Evidence of atmospheric nanoparticle formation from emissions of marine microorganisms, Geophys. Res. Lett., 43, 6596–6603, https://doi.org/10.1002/2016gl069389, 2016.

Sherwen, T., Evans, M. J., Carpenter, L. J., Andrews, S. J., Lidster, R. T., Dix, B., Koenig, T. K., Sinreich, R., Ortega, I., Volkamer, R., Saiz-Lopez, A., Prados-Roman, C., Mahajan, A. S., and Ordóñez, C.: Iodine's impact on tropospheric oxidants: a global model study in GEOS-Chem, Atmos. Chem. Phys., 16, 1161–1186, https://doi.org/10.5194/acp-16-1161-2016, 2016.

Sherwen, T., Chance, R. J., Tinel, L., Ellis, D., Evans, M. J., and Carpenter, L. J.: A machine-learning-based global sea-surface iodide distribution, Earth Syst. Sci. Data, 11, 1239–1262, https://doi.org/10.5194/essd-11-1239-2019, 2019.

Spokes, L. J. and Liss, P. S.: Photochemically induced redox reactions in seawater, 2. Nitrogen and iodine, Mar. Chem., 54, 1–10, https://doi.org/10.1016/0304-4203(96)00033-3, 1996.

Teiwes, R., Elm, J., Bilde, M., and Pedersen, H. B.: The reaction of hydrated iodide $I(H_2O)^-$ with ozone: a new route to IO_2^- products, Phys. Chem. Chem. Phys., 21, 17546, https://doi.org/10.1039/c9cp01734h, 2019.

Truesdale, V. W. and Spencer, C. P.: Studies on the determination of inorganic iodine in seawater, Mar. Chem., 2, 33–47, https://doi.org/10.1016/0304-4203(74)90004-8, 1974.

Truesdale, V. W. and Moore, R. M.: Further studies on the chemical reduction of molecular iodide added to seawater, Mar. Chem., 40, 199–213, https://doi.org/10.1016/0304-4203(92)90023-4, 1992.

Truesdale, V. W., Bale, A. J., and Woodward, E. M. S.: The meridional distribution of dissolved iodine in near-surface waters of the atlantic ocean, Prog. Oceanogr., 45, 387–400, https://doi.org/10.1016/s0079-6611(00)00009-4, 2000.

Truesdale, V. W.: On the feasibility of some photochemical reactions of iodide in seawater, Mar. Chem., 104, 266-281, https://doi.org/10.1016/j.marchem.2006.12.003, 2007.

Tsunogai, S. and Sase, T.: Formation of iodide-iodine in ocean, Deep-Sea Res., 16, 489–496, https://doi.org/10.1016/0011-7471(69)90037-0, 1969.

Tsunogai, S.: Iodine in the deep water of the ocean, Deep-Sea Res., 18, 913–919, https://doi.org/10.1016/0011-7471(71)90065-9, 1971.

van Bergeijk, S. A., Javier, L. H., Heyland, A., Manchado, M., and Canavate, J. P.: Uptake of iodide in the marine haptophyte *Isochrysis* sp. (T. ISO) driven by iodide oxidation, J. Phycol., 49, 640–647, https://doi.org/10.1111/jpy.12073, 2013.

van Bergeijk, S. A., Hernandez, L., Zubia, E., and Canavate, J. P.: Iodine balance, growth and biochemical composition of three marine microalgae cultured under various inorganic iodine concentrations, Mar. Biol., 163, 640–647, https://doi.org/10.1007/s00227-016-2884-0, 2016.

Vogt, M., O'Brien, C., Peloquin, J., Schoemann, V., Breton, E., Estrada, M., Gibson, J., Karentz, D., Van Leeuwe, M. A., Stefels, J., Widdicombe, C., and Peperzak, L.: Global marine plankton functional type biomass distributions: Phaeocystis spp., Earth Syst. Sci. Data, 4, 107–120, https://doi.org/10.5194/essd-4-107-2012, 2012.

Waite, T. J. and Truesdale, V. W.: Iodate reduction by isochrysis galbana is relatively insensitive to de-activation of nitrate reductase activity – are phytoplankton really responsible for iodate reduction in seawater?, Mar. Chem., 81, 137–148, https://doi.org/10.1016/s0304-4203(03)00013-6, 2003.

Waterbury, J. B., Watson, S. W., Valois, F. W., and Franks, D. G.: Biological and ecological characterization of the marine unicellular cyanobacterium synechococcus, in: Photosynthetic picoplankton, edited by: Platt, T. and Li, W. K. W., Can. B. Fish. Aquat. Sci., 214, 71–120, 1986.

Wong, G. T. F., Brewer, P. G., and Spencer, D. W.: Distribution of particulate iodine in atlantic ocean, Earth Planet. Sci. Lett., 32, 441–450, https://doi.org/10.1016/0012-821x(76)90084-4, 1976.

Wong, G. T. F. and Cheng, X. H.: Dissolved organic iodine in marine waters: Role in the estuarine geochemistry of iodine, J. Environ. Monit., 3, 257–263, https://doi.org/10.1039/b007229j, 2001.

Wong, G. T. F. and Hung, C. C.: Speciation of dissolved iodine: Integrating nitrate uptake over time in the oceans, Cont. Shelf Res., 21, 113–128, https://doi.org/10.1016/s0278-4343(00)00086-8, 2001.

Wong, G. T. F., Piumsomboon, A. U., and Dunstan, W. M.: The transformation of iodate to iodide in marine phytoplankton cultures, Mar. Ecol.-Prog. Ser., 237, 27–39, https://doi.org/10.3354/meps237027, 2002.

Wong, G. T. F. and Zhang, L.-S.: The kinetics of the reactions between iodide and hydrogen peroxide in seawater, Mar. Chem., 111, 22–29, https://doi.org/10.1016/j.marchem.2007.04.007, 2008.

Zic, V., Caric, M., and Ciglenecki, I.: The impact of natural water column mixing on iodine and nutrient speciation in a eutrophic anchialine pond (rogoznica lake, croatia), Estuar. Coast. Shelf Sci., 133, 260–272, https://doi.org/10.1016/j.ecss.2013.09.008, 2013.